Chapter 3

Materials and methods

3.1 Material selection

Fe-Mn-Al-C alloy steels are designed to achieve a balance of reduced density, high strength, and excellent ductility. This type of alloy is particularly characterized as austenitic based Fe-Mn-Al-C steels in which ferrite phase and carbide precipitates are relatively very low. Below is an elaboration on range of mass percentage of each allying element to form austenite steel with specific microstructural and mechanical features.

a. Aluminium (7% - 11%):
   - Reduces density (15%-20%) and stabilizes austenitic phases.
   - Prevents ferrite and carbide formation.

b. Carbon (0.7% - 1.2%):
   - Balances strength and ductility.

c. Manganese (20% - 30%):
   - Stabilizes the austenitic phase, enhancing ductility (>60%) and toughness without promoting brittle carbides.

On the basis of above mentioned features the two best suited composition for MAF processes are shown in Table 6.

Table 6: Selected compositions (mass %).

Element	Mn	Al	C	Si	Cr	Ni	Fe
Fe-30Mn-9Al-0.8C (S1)	30.19	9.15	0.8	0.16	0.15	0.09	Bal.
Fe-20Mn-10Al-1C (S2)	20.10	10.17	1	0.18	0.17	0.11	Bal.

3.2 Vacuum induction melting

Vacuum induction melting is a process used to produce high-purity metal alloys by melting the raw materials in a vacuum environment. This method minimizes contamination and allows precise control over the chemical composition and microstructure of the alloy. The vacuum induction melting setup for making the alloy steels is shown in Fig. 8. The melting facility is provided by the Advance Research Centre for Iron and Steel Making in the Department of Metallurgical Engineering, IIT(BHU), Varanasi.

Fig. 8: Vacuum induction melting furnace setup.

3.2.1 Raw materials for melting

For producing S1 and S2 steels, the following raw materials are used:

1. Ferro carbon
2. Pure aluminium
3. Electrolytic manganese
4. Ferro manganese

3.2.2 Melting procedures

A 2.5 kg ingot of S1 and an ingot with same weight of S2 steels are prepared using the vacuum induction melting process. The specific process sequences are critical for achieving the desired alloy properties.

Process optimization sequence:

Step 1 - Initial charging:

The process starts by adding ferro carbon and pure aluminium to the induction furnace.

Step 2 - Vacuum creation:

A high vacuum of $< 10^{-3}$ mbar is created to eliminate any atmospheric contamination.

Step 3 - Melting phase:

The furnace is activated, and the charge is melted at approximately 1580℃ for 15 minutes.

Step 4 - Pressure adjustment:

The vacuum is blocked, and argon gas is injected into the melt chamber to achieve a pressure of 600 mbar.

Step 5 - Addition of manganese:

Electrolytic manganese and ferro manganese are added to the melt at ≈1550℃, ensuring the chamber remains closed to maintain the inert atmosphere.

Step 6 - Mixing and pouring:

The molten metal is thoroughly mixed to achieve a uniform composition.

The molten alloy is then poured into a copper mould to form the final ingot.

3.3 Thermomechanical processing

Step 1: Homogenization

- The materials of dimensions 45 mm x 25 mm x 20 mm are homogenized at 1200℃ in a tube furnace.

- It is done to reduce the effect of micro-segregation and to produce uniform distribution of elements.

Step 2: Biaxial hot forging

- The homogenized materials are then hot forged between 1200℃ to 900℃ with intermediate heating and then WQ.
- The materials are forged in two directions so that more 60 % deformation could be achieved.
- It is done to break the dendritic structure.
- The hot forging has been carried out on a power hammer machine.

The hot forged and WQ S1 and S2 steels are designated as FS1 and FS2, respectively.

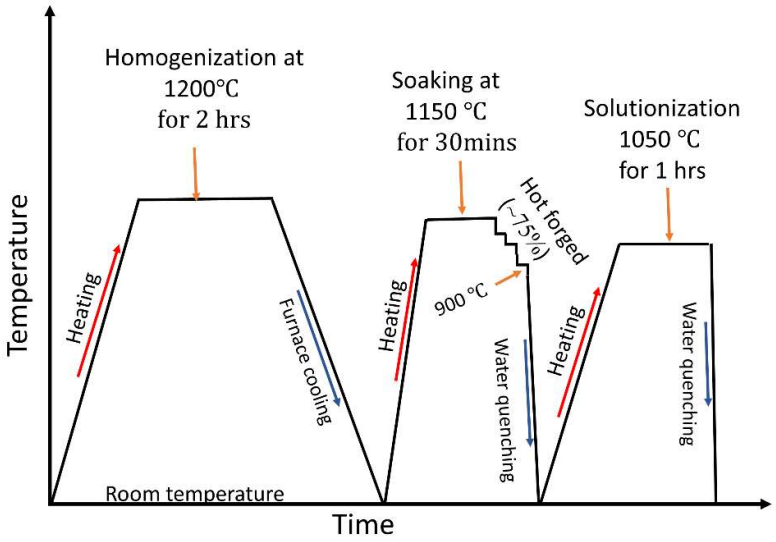

Fig. 9: Thermomechanical cycle.

Step 3: Solutionization

- The forged material is then solutionized at 1050℃ for 1 hour and WQ.
- It is done to dissolve some precipitates and create a new solid solution phase.

The solutionized and WQ S1 steel and S2 steel are designated as SS1 and SS2 respectively.

3.4 Die design for multiaxial forging

3.4.1 Detailed description of the die material and die drawing

Die material: - H13 Hot-worked tool steel.

H13 is a chromium-molybdenum-vanadium hot-worked tool steel known for its excellent combination of high toughness and high resistance to thermal fatigue cracking. It is widely used in the manufacture of dies for hot working processes due to its superior mechanical properties. The steel has been purchased from Kumar Enterprise Pvt. Ltd., Kanpur. The supplier provided the material in an unhardened condition. Purchasing the steel in an unhardened state is advantageous for the initial machining and fabrication processes as it allows for easier shaping and dimensioning of the material before it undergoes hardening treatments. The detail die drawings with specifications are given in Fig.10. The fabrication of the die was carried out at Anand Tools Pvt. Ltd., Kanpur. Anand Tools is known for its expertise in precision tooling and fabrication.

Steps of Heat treatment:

Preheating

- Heating the die parts at 200℃/ hr to 650^0C (total heating time = 3.25 hrs. (approx.))
- Soaking it at 650 ℃ for 30 mins for uniform temperature distribution.
- Then again heating the material at 200℃/hr to 850℃. (total heating time = 1 hr. (approx.))
- Soaking it at 850℃ for 30 mins for temperature equalization

Austenitizing

- Heating the preheated parts at 200℃/hr to 1050℃ (total heating time = 1 hr. (approx.))
- Soaking it at 1050℃ for 1.5 hr.
- Cooling the austenitized parts by oil quenching.

- When sample color becomes black, it is put in air and cooled till the sample reaches 50℃.

Tempering

- After hardening, tempering of the steel is done immediately.
- Tempering it at 540℃ for 1 hr. per inch thickness, 3 hrs. per 3 inches thickness and then it is cooled in air to room temperature.

Machining and finishing

- To achieve accurate dimensions and a high-quality surface finish, the die is polished using diamond polishing technique. This process provides a superior finish and ensures that the die meets the required specifications.
- Finally, the grooves in the die are chrome-coated. This chrome coating enhances the wear resistance and durability of the grooves, ensuring that they maintain their precise dimensions and functionality during the hot working process.

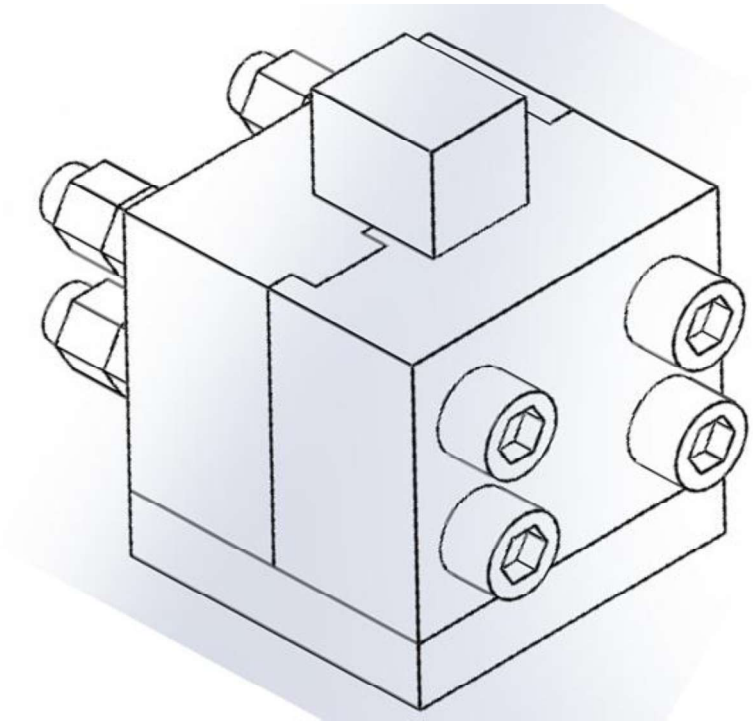

(a)

Fig. 10: continued..

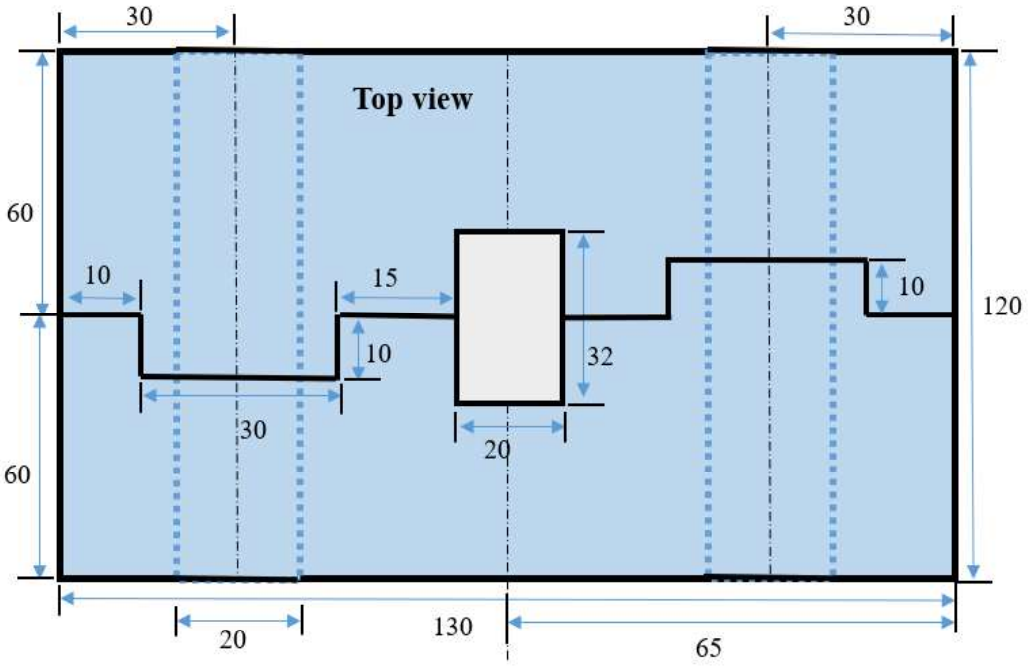

(b)

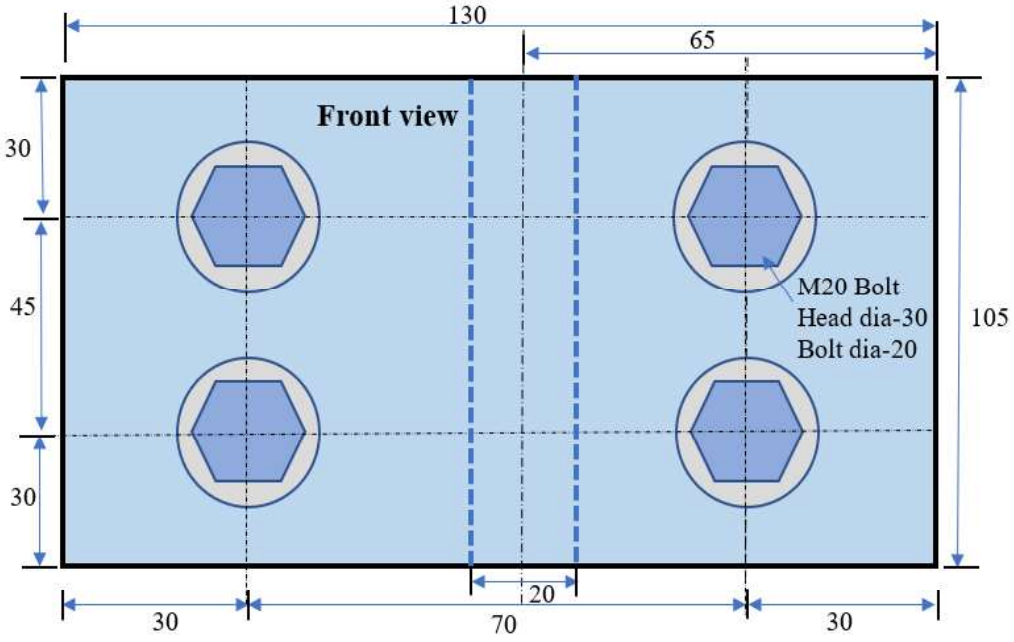

(c)

Fig. 10: continued..

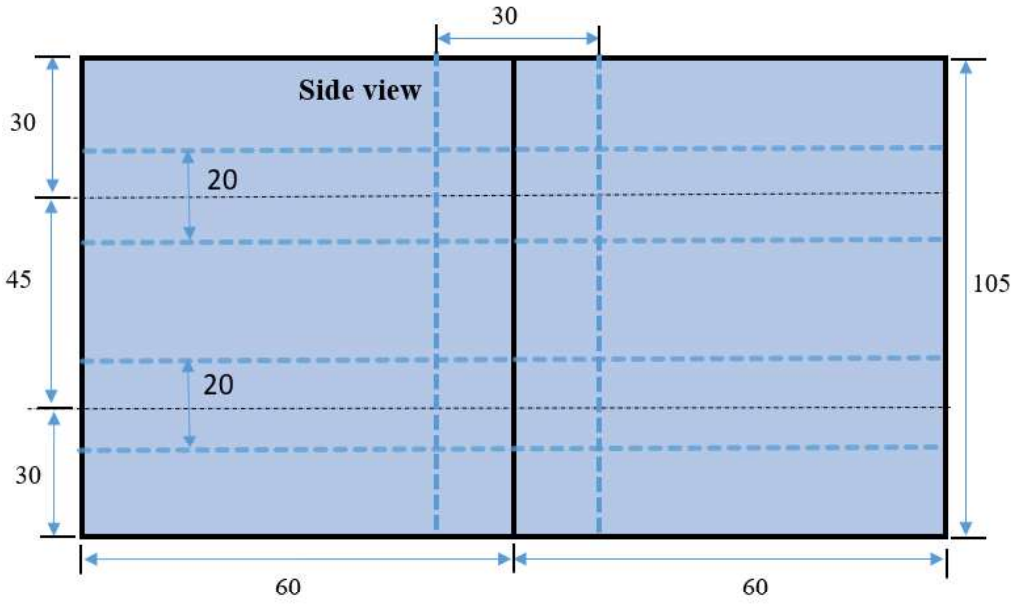

(d)

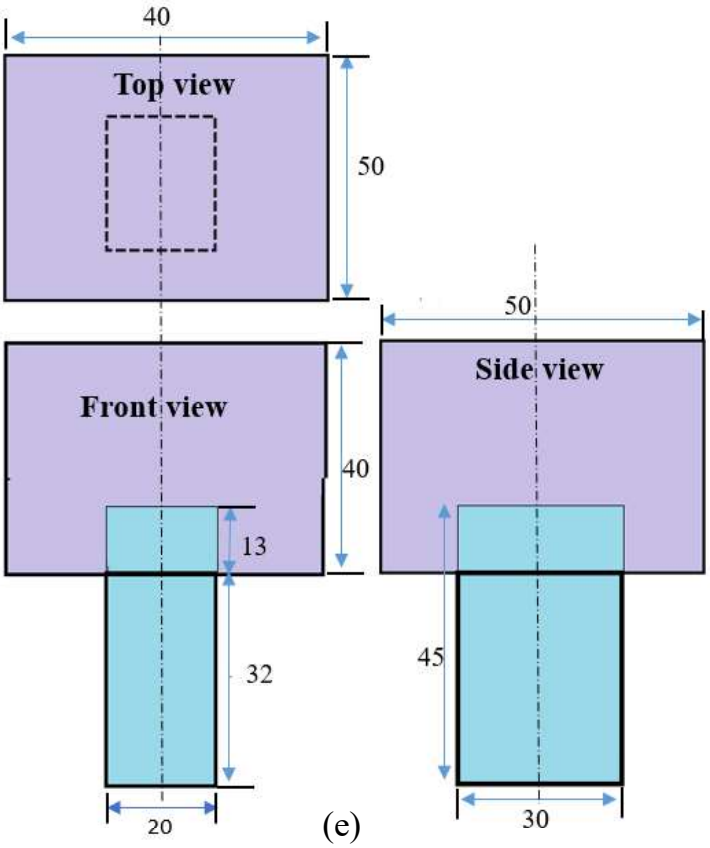

(e)

Fig. 10: continued..

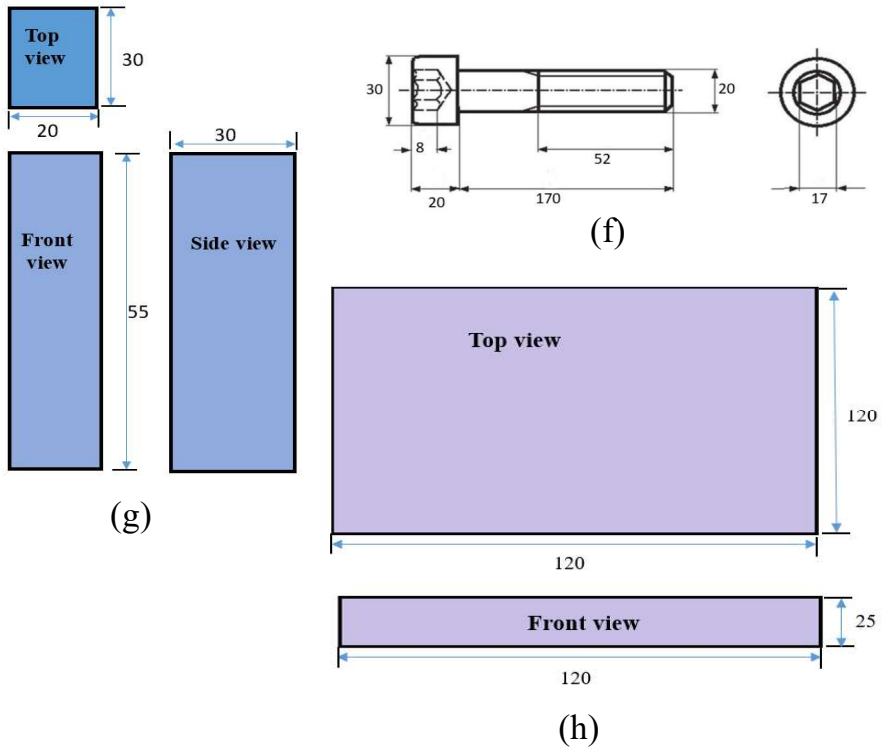

Fig. 10: Specification of die setup design (a) isometric view of the MAF die, (b) die top view, (c) die front view, (d) die side view, (e) punch and punch head, (f) bolt, (g) spacer, and (h) base plate.

3.5 Multiaxial forging process

The MAF is carried out along three orthogonal directions on a 100-ton hydraulic press as shown in Fig. 11a. Workpieces of 30 mm x 20 mm x 20 mm dimensions are cut from the solutionized billets designated as MAF-0. These MAF-0 workpieces are multiaxially forged at 250°C in the die given in Fig. 11b. The orientation and rotation of the workpiece at various stages of a complete cycle of MAF are given in Fig. 11c. All samples have been thoroughly lubricated with MoS_2 before pressing. Prior to MAF, the sample and die are heated to 250°C and soaked for two hours. The steel with the specified composition has the highest malleability between 150°C to 450°C below the recrystallization temperature, and

therefore, the tests are carried out at 250℃ (warm deformation circumstances). It is worth mentioning that the precipitation of carbides develops when the Fe-Mn-al-C low-density steel is deformed at temperatures higher than 450℃, increasing the material's hardness and decreasing its ductility [14], [165]. The ram has moved at a steady speed of 1 mm/s. MAF is performed by compressing the billet in three mutually perpendicular directions, which is referred to as one cycle.

For the first pass, the MAF-0 workpiece (step i) is pressed along the y-axis, where material flows along the x-axis and the z-axis remains in a constrained direction. MAF-0 workpiece after the first pass is designated as MAF-1. A single pass of MAF induces 33% normal strain, for which the equivalent strain is calculated to be 0.468 [24], reducing the initial sample height from 30 mm to 20 mm. The MAF-1 workpiece is then taken out and rotated by 90° about the y-axis (steps ii-iii) and z-axis (steps iii-iv), respectively, in clockwise and anticlockwise directions. The rotated MAF-1 workpiece is then pressed along the x-axis (steps iv-v) while the flow is in the z-axis and the y-axis is constrained.

MAF-1 workpiece after the second pass is designated as MAF-2. MAF-2 workpiece is taken out from the die and rotated by 90° about the x-axis (steps v-vi) and y-axis (steps vi-vii), respectively, in clockwise and anticlockwise directions. The rotated MAF-2 workpiece is pressed along the z-axis (steps vii-viii) while the flow is in the y-axis, and the x-axis is constrained in direction. MAF-2 workpiece after the third pass is designated as MAF-3. MAF-3 workpiece is taken out from the die and is rotated by 90° about the z-axis (steps viii-ix) and y-axis (steps ix-x), respectively, in clockwise and anticlockwise directions. The rotated MAF-3 reaches the original orientation and is ready for the next pass. The MAF of the workpiece in the above sequence by the steps from i-x completes one cycle of deformation, at the end of which the workpiece gets its original orientation. The deformation on the workpiece is repeated by steps i-x for subsequent cycles. However, the

material could be deformed up to 5 passes without any crack. The multiaxially forged sample with sample reference axes, i.e., the pressing direction, the constrained direction, and the flow direction are given in Fig. 11. The workpiece failed during the sixth pass of MAF. The workpiece after five passes of MAF is designated as MAF-5.

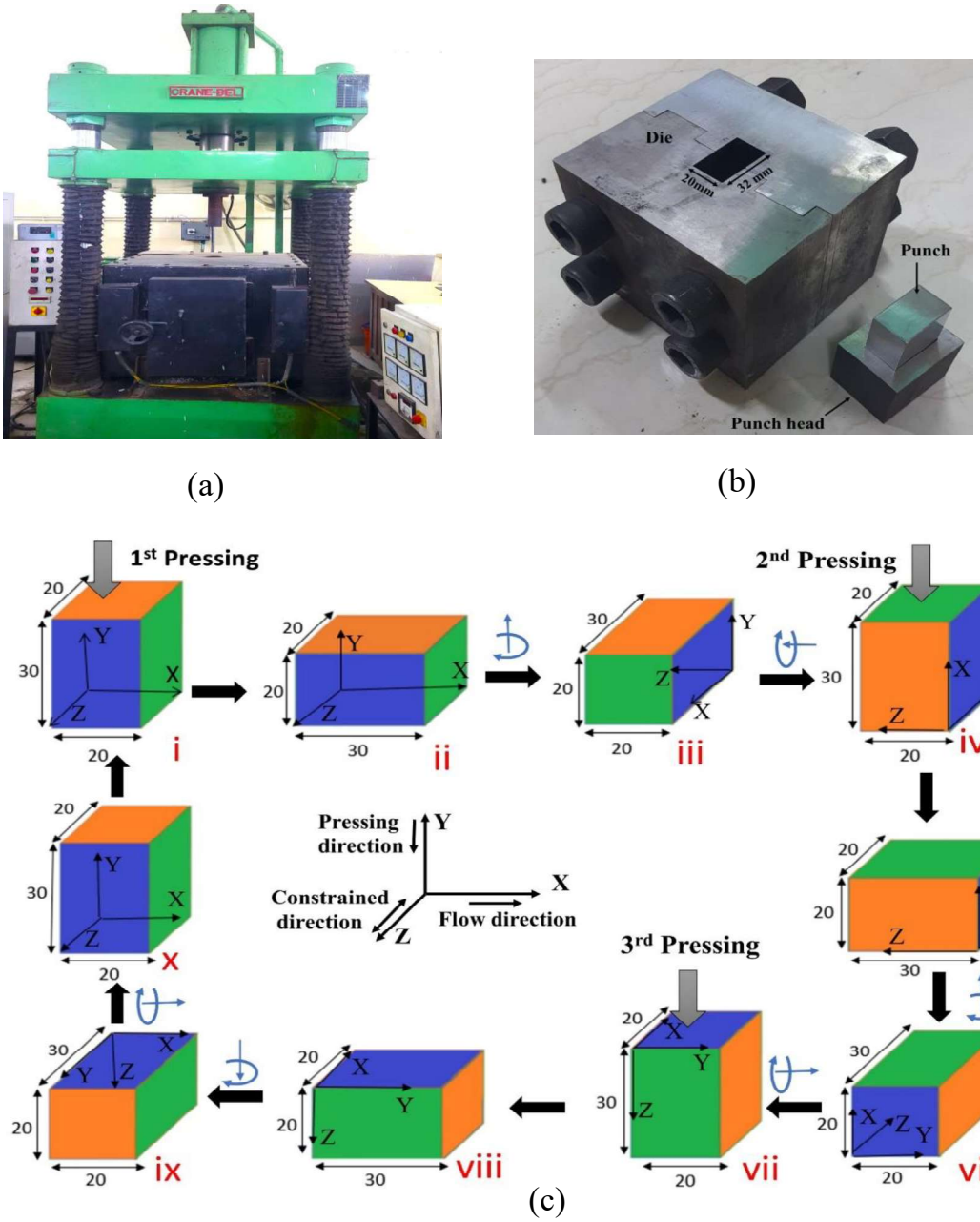

Fig. 11: (a) Testing setup of hydraulic press, (b) die used during MAF, (c) schematic diagram of orientation and rotation of workpiece at various stages of a complete cycle of MAF.

3.6 Material characterization

3.6.1 Composition analysis

The solutionised and WQ billet are taken for chemical analysis and the mass fraction of each alloying element is regarded as the actual chemical composition of MAF-0. The carbon concentrations are assessed through combustion infrared detection analysis, employing a LECO CS744 analyzer. Concentrations of other elements are determined through the application of wet chemical analysis. The MAF-0 samples are utilized for micro-mechanical examination of the proposed composition.

3.6.2 Optical microscopy

Microstructural studies of all the MAF-0, MAF-1, MAF-3, and MAF-5 specimens of SS1 steel and MAF-0, MAF-1 and MAF-2 of SS2 steel are carried out along the width region employing an optical microscope (Leica DM 2500 M). The specimens are polished using standard metallographic techniques, followed by etching with 2 % nital solution for 2 mins to reveal its microstructural features.

3.6.3 X-ray diffraction

Phase identification of the processed specimens is carried out with the help of a Panalytical Emperean X-ray diffractometer equipped with Co-Kα radiation (λ = 1.54056 Å). The instrument operates at an operating voltage of 40 kV, a current of 40 mA. The specimens are analyzed with the 2θ range varying from 40° to 120° and the step size of 0.02°. The data generated by XRD are analyzed using X'Pert High Score Plus software to identify the phases present in the processed specimens. Further, the lattice parameters of ferrite and austenite phases as well as the precipitates are also determined from the same software.

3.6.4 Electron back scattered diffraction

EBSD analyses are performed to investigate the grain boundary character distribution for both LAGBs and HAGBs, inverse pole figures and Kernel average misorentation distribution for each pass. Specimens for EBSD are sectioned in 12 mm x 10 mm x 4 mm dimension from the deformed sample and prepared through standard metallographic polishing procedures, with electro-polishing (80% ethanol and 20% perchloric acid) as the final step. The electropolished specimens are mounted on carbon tape on the specimen holder and examined in a field emission SEM. The EBSD data from the scan surface of each specimen are analyzed using TSL-OIM (version 7.2).

3.7 Tensile testing

3.7.1 Tensile test of solutionised and WQ samples

Flat and round tensile specimens have been machined according to ASTM E8-04 from WQ ingot and their dimensions are shown in Figs. 12c and 13c, respectively. The images of the prepared samples for tensile tests at different strain rates and at different elevated temperatures are shown in Figs. 12b and 13b, respectively. Tensile tests at four different strain rates (10^{-4},10^{-3},10^{-2} and 10^{-1} s^{-1}) at room temperature have been conducted using a servo-hydraulic high speed tensile testing machine. Tensile deformations at elevated temperatures (150°C, 300°C and 450°C) with strain rate of 4.4 x 10^{-3} s^{-1} have been conducted on INSTRON's hydraulic universal testing machine. The images of the tensile testing machines are shown in Figs. 12a and 13a. The yield strength, ultimate tensile strength and total elongation are evaluated from the stress-strain curves obtained from tensile tests.

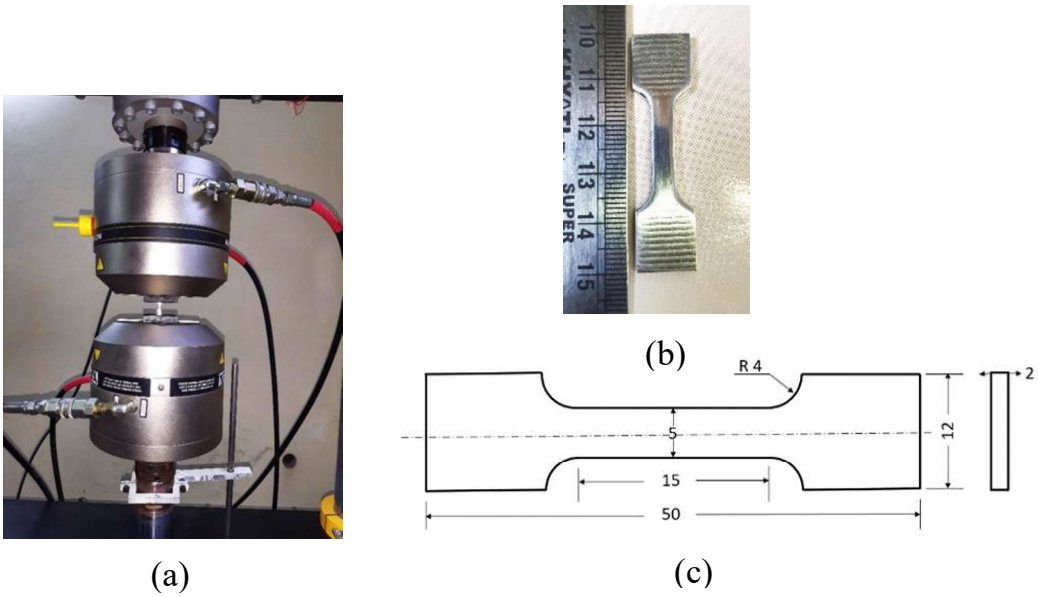

Fig. 12: (a) Loading assembly on servo hydraulic testing machine, (b) the prepared sample and (c) the dimensions (in mm) of flat tensile sample.

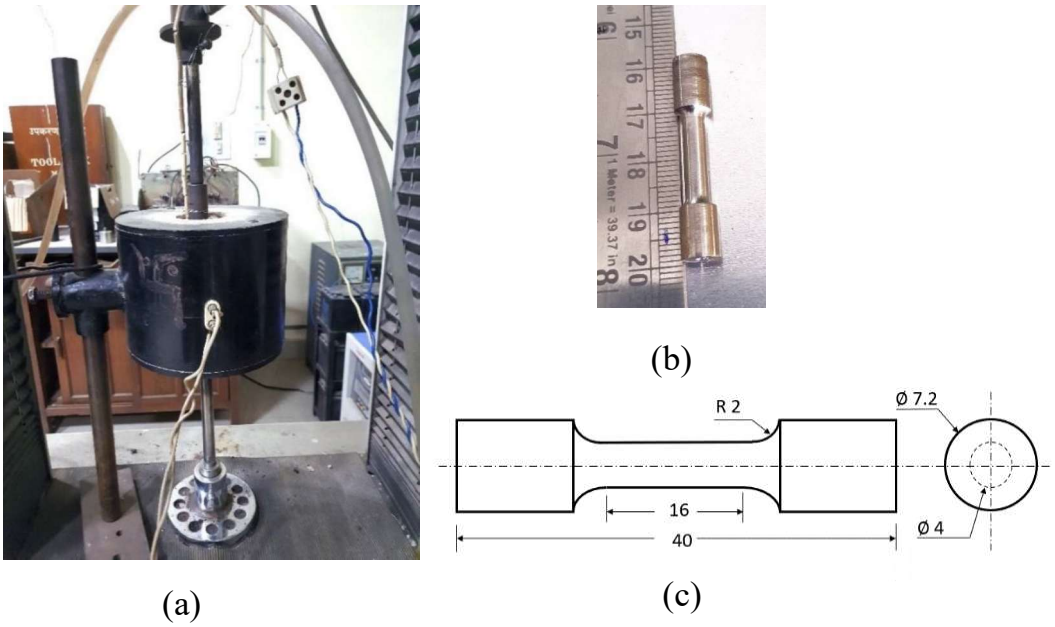

Fig. 13: (a) Loading assembly on INSTRON hydraulic testing machine, (b) the prepared sample and (c) the dimensions (in mm) of round tensile sample.

3.7.2 Tensile tests of multiaxially forged workpiece

The tensile tests are conducted to investigate the effect of multi direction forging on the tensile strength after each MAF pass. Miniature round tensile samples at MAF-0, MAF-1, MAF-3, and MAF-5 of S1 steel and MAF-0, MAF-1, and MAF-2 of S2 steel have been cut from the located area of MAF sample as shown in Fig. 14a. The dimensions of tensile sample are shown in Fig. 14b. These samples are tested on hydraulic universal testing machine of INSTRON with a strain rate of 1 x 10^{-3} s^{-1} at room temperature. Two round tensile samples have been taken from each chosen MAF pass to confirm reliability.

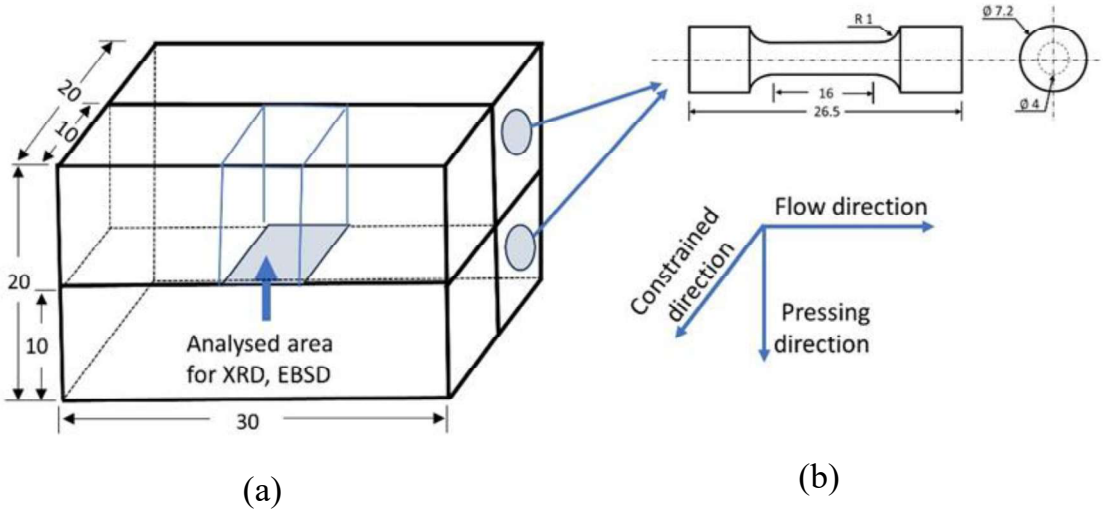

Fig. 14: (a) Location of samples taken for various testings/characterization from MAF workpiece, (b) Schematic diagram of tesile sample. All dimensions are in mm.

At the end of tensile test, the two broken halves are placed properly and increase in plastic length is measured physically. Using this data, the amount of elastic length is estimated which has elastic length components from sample as well as from the machine. The elastic length is subtracted from each elongation data and the resultant value is reported as increase

in plastic length of the gauge which is utilized for calculation of plastic strain. Only plastic strain is calculated from the increase in displacement which is divided by the gauge length.

3.8 Residual stress measurement

3.8.1 Residual stress measurement procedure

Each electropolished sample is placed on the cradle such that the flow direction should be parallel to the plane containing incident and diffracted beam as well as to diffracting plane as shown in Fig. 15. A phase scan in line-focus was performed using incident and diffracted optics of fixed divergence slit and fixed anti-scatter slit, respectively (Fig. 15a), at 45 kV voltage and 40 mA current, at the scan rate of 2°/min adopting Cu target for each polished sample to know the diffraction angles (2θ). The incident optics and diffracted optics are changed to a poly-capillary lens and parallel plate collimator, respectively, for point focus. A manual scan using a direct beam is performed without β filter within ±0.5° of 2θ axis range to correct its offset.

A combination of manual scans is performed to correctly align the sample and offsets in ω and χ. A set of manual scans (Z scan, ω scan, fine Z scan, fine ω scan and χ scan) is performed to know and correctly position the surface of the sample (as indicated by sample reference axes in Fig. 15b) parallel to direct beam path, ω offset, confirming Z, ω and χ offsets. The respective higher diffraction angle peaks at 87.95°, 87.80°, 88.26°, and 87.95° with ±2° range corresponding to (311) plane for the MAF-0, MAF-1, MAF-3 and MAF-5 of S1 steel are utilized for Gonio scan to know correctly its position.

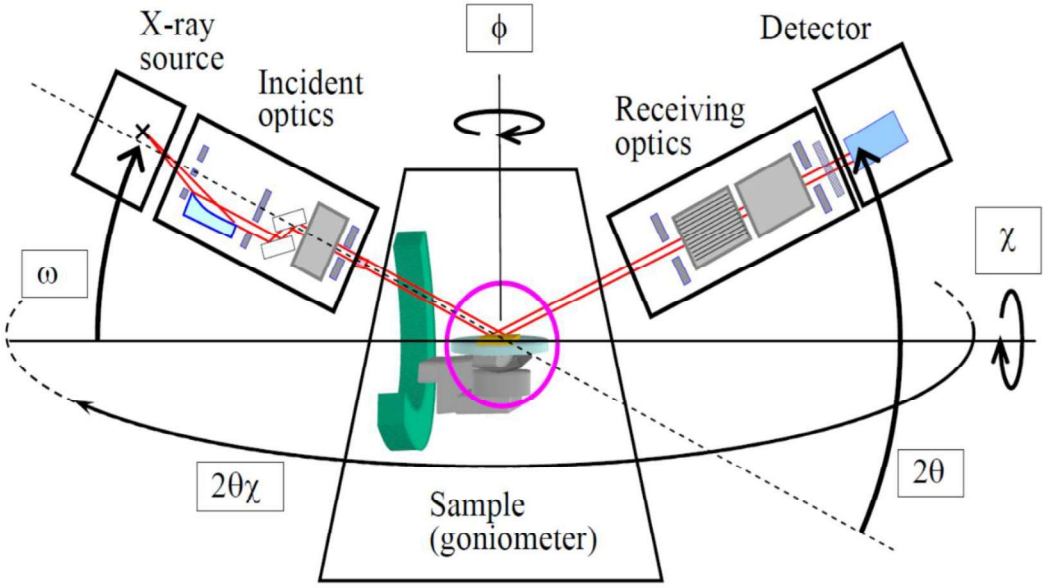

(a)

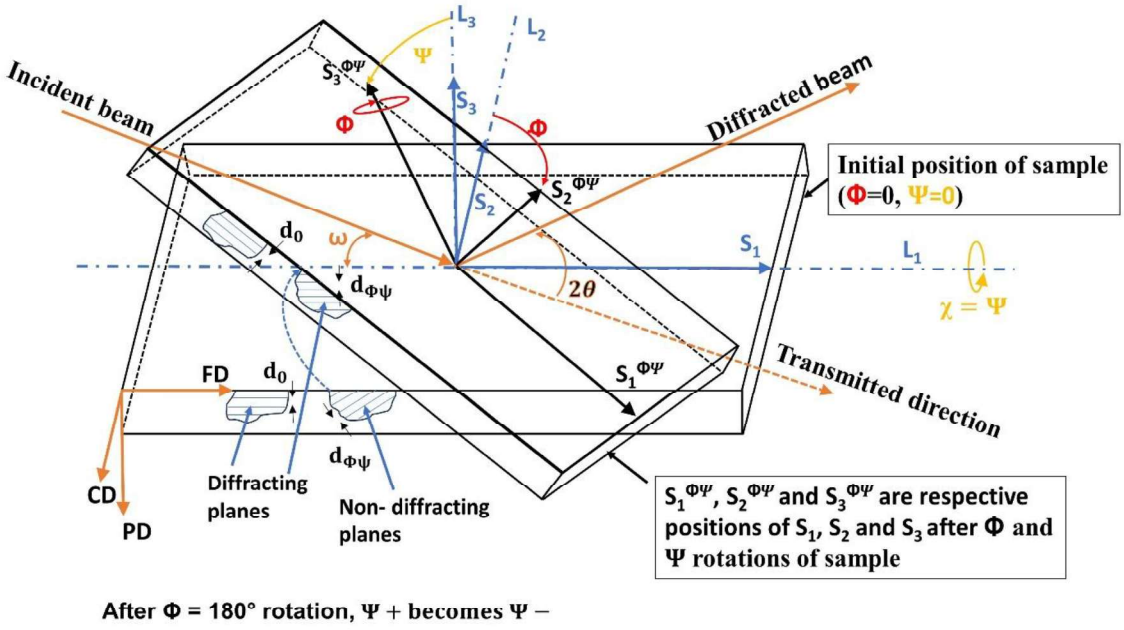

(b)

Fig. 15: (a) Angle and axis rotation in Empyrean System (b) schematic diagram of sample with sample reference axes (S_1, S_2, S_3) and laboratory/beam reference axes (L_1, L_2 and L_3) and diffracting planes.

The scan rate for Chi-scan (residual stress measurement) is decided by the FWHM of Gonio scan/8 and a time per step to get about 100 steps in the selected 2θ ±2° range. The Chi-scan method is performed for the selected sample at 45 kV voltage and 40 mA current using Cu Kα=1.5406 Å and the scan rate of 0.048°/s for the selected 2θ range and the Chi angle range of 0°-90° with a positive (Φ =0°-180°) and pseudo negative tilts (Φ =180°-360°). Selected two-theta scan data are collected at the Φ angles of 0°, 45°, 90°,180°, 225° and 270° and $\sin^2\chi$ step size of 0.09 in the range 0-0.9. Two-theta scan data at the Phi angles of 0°, 45°and 90° are utilized for biaxial stress analysis, scan data at Phi angles of 0° and 90° are utilized to correct error in biaxial stress analysis and Phi angles of 0°, 45°, 90°,180°, 225° and 270° are used for triaxial stress analysis. S_1, S_2 and S_3 are three orthogonal sample reference axes, and initially, S_1, S_2 and S_3 are parallel to three orthogonal laboratory/beam axes, L_1, L_2 and L_3, respectively. Where L_1 is in a plane containing the incident and diffracted beam, L_1 & L_2 are perpendicular to each other and parallel to the diffracting crystallographic plane, and L_3 is normal to it. Here, ω is the incident angle, Φ is the rotation angle of the sample about its surface normal S_3, and χ is the rotation angle of the sample about L_1. With χ rotation, planes (hkl) (of similar Millar indices) of deviated d values (due to strain) within the given 2θ range are coming in diffracting conditions. Here, for all conditions, χ= ψ. The $\sin^2\psi$ method is adopted for strain measurement. The amount of strain is calculated from the deviation in 2θ or in d value.

3.8.2 Residual stress analysis

A single-wavelength X-ray beam strikes the surface, causing a diffraction beam to arise at a diffraction angle of 2 theta (2θ) that is connected to a specific crystalline lattice plane indicated by (hkl). The d-spacing (d) of the (hkl) plane is determined by using Bragg's formula $n\lambda = 2d\sin\theta$, where λ stands for the X-ray wavelength. If d is the distance between

the lattice planes measured in the direction, the strain can be represented in terms of changes in the linear dimensions of the crystal lattice. The normal strain (ε_N) of the surface of the sample is measured by the ratio of the difference in interplanar spacing (or Δd) between the d of the crystallographic plane (d_{hkl}) parallel to the surface of the multiaxially forged sample and the d of the annealed sample (d_0) to the d_0, which is given by the Eq. (3).

$$\varepsilon_N = \frac{\Delta d}{d_0} = \frac{d_{hkl} - d_0}{d_0} \quad (3)$$

By tilting the sample within the diffractometer, for an angle of ψ (=χ) after the rotation of the sample about its surface normal by an angle Φ, the measured strain $(\varepsilon_{33})_{\Phi\Psi}$ along the normal direction of the (hkl) plane (the plane has come under diffraction conditions, ε_{33} is the strain on L_3, plane and along L_3 direction) is calculated by using Eq. (4) similar to Eq. (3).

$$(\varepsilon_{33})_{\Phi\Psi} = \frac{\Delta d}{d_0} = \frac{d_{\Phi\Psi} - d_0}{d_0} \quad (4)$$

Where, $d_{\Phi\Psi}$ & d_0 are interplanar spacing of the rotated plane (hkl) of strained crystal and annealed crystal, respectively. The measured strain $(\varepsilon_{33})_{\Phi\Psi}$ is transformed to ε_{pq} in the sample coordinate system with the help of $a_{3m}.a_{3n}$ coefficients found from the tensor transformation given by Eq. (5) [25]:

$$(\varepsilon_{33})_{\Phi\Psi} = a_{3p}a_{3n}\varepsilon_{pq} \quad (5)$$

Where, ε_{pq} is the strain in the p plane and in the q direction of the sample; a_{3p}, a_{3q} are the direction cosines between L_3 & S_p and L_3 & S_q, respectively, where for plane normals of sample, subscript p=1,2,3 and for sample axes, subscript q=1,2,3

The direction cosine matrix a_{ij} for transforming strain along laboratory axes to sample reference axes is given by Eq. (6)

$$a_{ij}=\begin{vmatrix} \cos\Phi\cos\Psi & \sin\Phi\cos\Psi & -\sin\Psi \\ -\sin\Phi & \cos\Phi & 0 \\ \cos\Phi\sin\Psi & \sin\Phi\sin\Psi & \cos\Psi \end{vmatrix} \quad (6)$$

Here, row numbers i=1,2,3 denote laboratory axes, and columns j indicate sample axes (q=1,2,3) or plane normal (p=1,2,3).

Combining Eqs. (5) and (6), we get Eq. (7) for measured strain,

$$(\varepsilon_{33})_{\Phi\Psi} = \varepsilon_{11}\cos^2\Phi\sin^2\Psi + \varepsilon_{12}\sin 2\Phi\sin^2\Psi + \varepsilon_{22}\sin^2\Phi\sin^2\Psi + \varepsilon_{33}\cos^2\Psi + \varepsilon_{13}\cos\Phi\sin 2\Psi + \varepsilon_{23}\sin\Phi\sin 2\Psi \quad (7)$$

Assuming that the material is homogeneous and isotropic, the macroscopic stress σ_{pq} is calculated from the strain ε_{pq} using Hooke's law through Eq. (8)

$$\varepsilon_{pq} = \frac{1+\nu}{E}\sigma_{pq} - \delta_{pq}\frac{\nu}{E}\sigma_{kk} \quad (8)$$

Where ε_{pq}, and σ_{pq} are the strain and stress, respectively in p^{th} plane (p=1,2,3) and q^{th} direction (q=1,2,3). δ_{pq} represents Kronecker delta,δ_{pq} = 0 for p≠q, but δ_{pq}=1 when p=q. k is the dummy suffix and implies summation for all k.

Substituting Eq. (8) in Eq. (7), we get Eq. (9) for the measured strain $(\varepsilon_{33})_{\Phi\Psi}$ or $d_{\Phi\Psi}$ in terms of residual stress components:

$$(\varepsilon_{33})_{\Phi\Psi} = \frac{d_{\Phi\Psi}-d_0}{d_0} = \frac{1+\nu}{E}\{\sigma_{11}\cos^2\Phi + \sigma_{12}\sin 2\Phi + \sigma_{22}\sin^2\Phi - \sigma_{33}\}\sin^2\Psi + \frac{1+\nu}{E}\sigma_{33} - \frac{\nu}{E}(\sigma_{11}+\sigma_{22}+\sigma_{33}) + \frac{1+\nu}{E}\{\sigma_{13}\cos\Phi + \sigma_{23}\sin\Phi\}\sin 2\Psi \quad (9)$$

In Eq. (9), σ_{11}, σ_{22}, and σ_{33} are the normal stress components along sample reference directions S_1, S_2, and S_3, and planes perpendicular to it, respectively. σ_{12}, σ_{23}, and σ_{13} are shear stress components.

Eq. (9) is utilized for calculating residual stress analysis for both biaxial or triaxial state of stress.

3.9 Constitutive equations for flow stress

3.9.1 Johnson-Cook constitutive equation

The stress-strain behavior of metallic material depends on the strain, strain rate and temperature. The coupled effect of all deformation conditions can be represented by J-C constitutive model. Because of its simplicity, this model is widely used by researchers in numerical computation of material behavior and the model also requires less effort to determine equation constants. The model is expressed as follows:

$$\sigma_{eq} = (A + B\varepsilon^{n})\left[1 + Cln\left(\frac{\acute{\varepsilon}}{\acute{\varepsilon}_0}\right)\right]\left[1 - \left(\frac{T - T_r}{T_m - T_r}\right)^{m}\right] \quad (10)$$

Where, σ_{eq} is equivalent stress, A is initial yield strength, B is strength coefficient, n is stain hardening exponent, C is strain sensitivity and m is thermal softening exponent, ε is the strain, $\acute{\varepsilon}$ is strain rate, $\acute{\varepsilon}_0$ is reference strain rate, T_r is room temperature, T_m is melting temperature. In Eq. (10), the 1st term within the parentheses corresponds to the dependence on strain, the 2nd term within square brackets corresponds to instantaneous strain-rate sensitivity, and the 3rd term within the square brackets corresponds to the temperature dependence of stress. True stress-strain data obtained from experimental tensile tests at various strain rate and temperature are used to determine the J-C constants.

3.9.2 Optimization of J-C parameters by genetic algorithm

The limitation of the parameters is that, they are accurate only for the condition under which the experiment is performed. Any alteration in experimental condition could mislead the result data. Therefore, optimization of material parameters is required when performing operations like metal forming to reveal the accurate description of deformation parameters. In this work, the J-C constants are optimized using optimization toolbox module of MATLAB software. A GA has been programed to optimize the J-C constants of low-density steel. The stress-strain data at different strain rates and temperatures at 43 strain

data points have been organized in a matrix form in MATLAB. GA is applied to evaluate material parameters by minimizing average absolute relative error (AARE) between the calculated and the experimental results. An objective function using least square-method is defined as follows [166]:

$$AARE = \frac{1}{N}\sum_{N=1}^{43}\left|\frac{\sigma_{exp} - \sigma_{pred}}{\sigma_{exp}}\right| \times 100\% \quad (11)$$

Where, σ_{exp} is the experimental flow stress, σ_{pred} is predicted flow stress (J-C flow stress), and N is the number of data points considered. Correlation coefficient (R^2) is used to show the strength of linear relationship of experimental and predicted data. The following expression for statistical measurement is used as [166]:

$$R^2 = 1 - \frac{\sum_{N=1}^{43}\left(\sigma_{exp} - \sigma_{pred}\right)^2}{\sum_{N=1}^{43}\left(\sigma_{exp} - \bar{\sigma}_{pred}\right)^2} \quad (12)$$

Where, $\bar{\sigma}_{pred}$ is mean flow stress of experimental values. A constrained optimization procedure has been adopted as shown in Fig. 16 to find the optimum constant values.

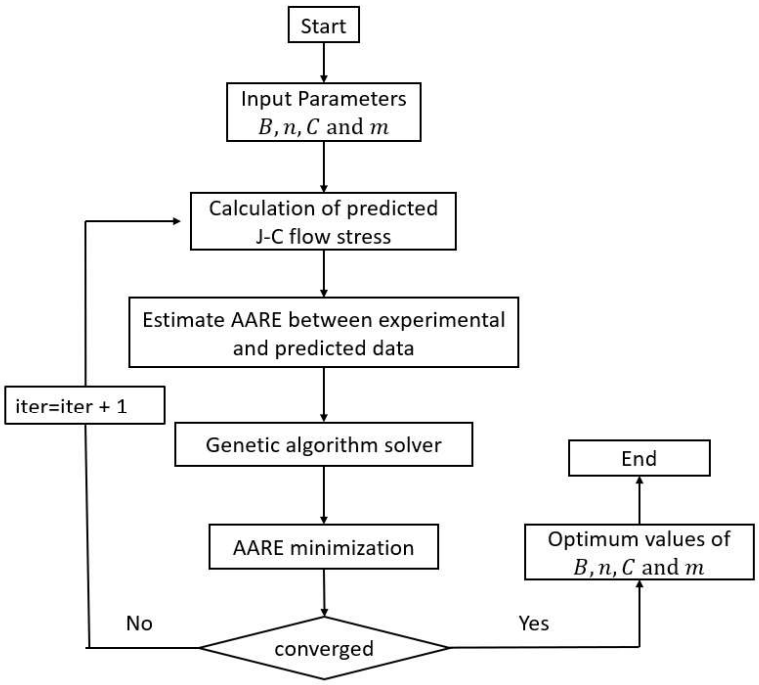

Fig. 16: Flow chart of optimization method.

3.10 Finite element method

3.10.1 Finite element simulation of tensile test

Two different 3D models have been built in ABAQUS to simulate the tensile test behavior for different working conditions. For replicating the stress-strain curves at a strain rate of 10^{-2} s^{-1} and at a temperature of 300℃, respectively, a flat and a round tensile specimens are modeled. The models have exactly the same dimensions as have been used in experiments. An 8-node linear hex element (C3D8R) is used to mesh the flat tensile model while, 4 node tetrahedral element (CD43) is used to mesh the round tensile model. The optimum mesh size has been determined by mesh convergence study for each model. For meshing purpose, the approximate element size at the gauge part is reduced to 0.5 mm for the flat sample and 1 mm for the round sample. A total of 2016 elements with 3429 nodes have been produced for the flat tensile model, compared to 2463 elements with 2898 nodes for the round tensile model. For boundary conditions, one end of the model is considered as fixed and the other end is displaced smoothly. For flat tensile model, simulation has been done at room temperature with cross-head speed of 9.6 mm/min to predict high strain rate (10^{-2} s^{-1}) behavior. On the other hand, for round tensile model, a predefined temperature field of 300℃ has been selected with cross-head speed of 4.3 mm/min for strain rate of 4.4×10^{-3} s^{-1}. Since the evaluated optimized parameters of J-C model predict more close material deformation behavior than the fitting parameters, these parameters are utilized in defining the material properties during the FE modelling.

3.10.2 Finite element simulation of multiaxial forging

As the material undergoes deformation and experiences varying stress, strain, and temperature levels, its behavior changes over time. The ABAQUS/Explicit finite element

package has been employed in this study to simulate the forging operation of low-density steel. A 3-D FE model with dimensions of 30 mm x 20 mm x 20 mm has been constructed to replicate the forging process accurately. To make sure that the simulation accurately depicts the process's dynamic and steady-state behaviour, the explicit dynamic technique has been used. The die and punch have been treated as discrete rigid bodies, whereas the workpiece has been treated as a deformable body. The mesh sensitivity analysis has been done to optimally calculate the mesh size of 0.6 mm. The overall number of hex components in the finished workpiece model is 41382 (C3D8R), with reduced integration and hourglass control. Employing an eight-node hex element is sufficient due to the symmetrical arrangement of the punch and die, which aligns with the direction of material flow. This choice of element reduces the maximum element count and minimizes the computational time required for the simulation. Regarding the boundary conditions used in the simulation, the punch undergoes a controlled displacement of 10 mm in the Y direction (height direction) while the die is tightly fixed. The layout of the die assures that the workpiece can only move in the X direction (flow direction), and the die wall's presence limits material flow in the Z direction (constrained direction).

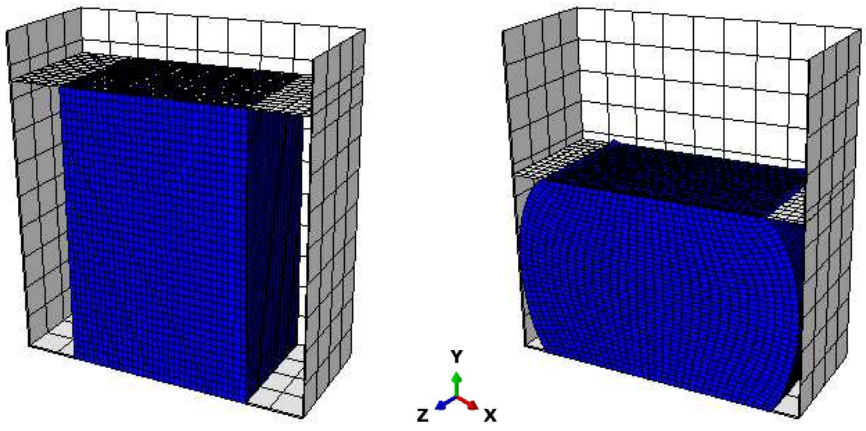

Fig. 17: Half-sectional view of 3-D finite element model of sample in a closed die before and after compression.

For this analysis, the overall contact between the workpiece and rigid bodies has been given a frictional coefficient of 0.15. The FE model is displayed in Fig. 17. Here, the 3-D FE model simulates the steady-state MAF process by mapping the distribution of the deformation fields from previous passes to the current ones. As shown in Fig. 17, the blank has been compressed in the height direction and expanded in the flow direction but does not deform in the constraint direction during the forging process because of the die constraint. In actual experimental practice, the sample is rotated, as shown in Fig. 11, but in simulation practice, the deformed model is fixed, and the punch and die are assembled in other directions to carry similar experimental boundary conditions.

Residual stress data for as-received sample (MAF-0) is served as the input to the FE model and thus it is acting as a pre-defined field to represent the initial condition of the material model. The FE model, incorporating elastic-plastic formulation, estimates residual stress through the application of sufficient relaxation time to recover elastic strain. The model is constructed in three steps: the first for progressive forging, the second for reducing punch kinetic energy to zero, and the third for punch return while accounting for elastic recovery in loading and flow directions. Relaxation is achieved by removing all boundary conditions and contact definitions between the sample and die during the cooling period.